Performance Evaluation of Solar-assisted Trigeneration System in Thermo-environmental Perspective

Meeta Sharma[1,*], Onkar Singh[2] and Anoop Kumar Shukla[1]

[1]*Mechanical Engg. Deptt., Amity School of Engg. & Tech., Noida (U.P.) – India*
[2]*Mechanical Engg. Deptt., Harcourt Butler Technical University, Kanpur (U.P.) – India*
E-mail: contactmeeta@yahoo.com; onkpar@rediffmail.com; shukla.anoophbti@gmail.com
[*]*Corresponding Author*

Received 12 May 2022; Accepted 19 July 2022;
Publication 09 December 2022

Abstract

Nowadays, the trigeneration systems are proving more promising than a combined cycle system. In terms of efficiency and reliability, these systems meet the typical requirements of cooling heating power in various applications. This work investigated the thermodynamic and environmental characteristics of a solar-based tri-generation system. The studied system consists of gas turbine and steam turbine modules along with heating and cooling provisions as per demand. The integrated system using parabolic trough collectors and also uses steam injected gas turbines for performance improvement. The overall performance of the proposed work is compared with and without a steam injection. The effect of integration of the solar cycle and steam injection for the trigeneration system is assessed. Further, carbon footprint rejected to the environment is also estimated. It is observed that the work

Distributed Generation & Alternative Energy Journal, Vol. 38_1, 41–66.
doi: 10.13052/dgaej2156-3306.3813

output and trigeneration efficiency improved, and the carbon footprint gets reduced in the range varying between 10–40% for the cases studied.

Keywords: Trigeneration system, steam injected gas turbine (STIG), solar cycle, thermodynamic analysis, parabolic trough collector (PTC).

Nomenclature

$\dot{Q}_i$	solar energy incident on the collector (kW)
$\dot{m}_f$	receiver's fluid mass flow rate (kg/s)
$h_{c,ca}$	cover and ambient, convection heat loss coefficient (W/m^{2}K)
$h_{r,ca}$	cover and ambient, radiation heat transfer coefficient, (W/m^{2}K)
$h_{r,cr}$	receiver and the cover, radiation heat transfer coefficient (W/m^{2}K)
A_{ap}	aperture area (m^2)
A_r	receiver pipe area (m^2)
c_p	specific heat at constant pressure (kJ/kg K)
c_{pf}	specific heat of heat transfer fluid (kJ/kg K)
emi_{CO2}	CO_2 emission rate (kg/kWh)
$E_{\varkappa_i}$	exergetic solar energy input (kW)
E_{xe}	solar collector exergy (kW)
F'	collector efficiency factor
F_r	collector heat removal factor
$\dot{q}_c$	cooling load, (kW)
$\dot{q}_h$	heating load, (kW)
Q_u	useful energy (kW)
T_e	exit temperature to receiver pipe (K)
T_i	inlet temperature to receiver pipe (K)
T_r	receiver temperature (K)
U_L	solar collector heat loss coefficient (W/m^{2}K)
U_o	overall heat transfer coefficient (W/m^{2}K)
W_{net}	net power generated, by the tri-generation system (kW)
Greek symbols	
η_{cc}	combustion chamber efficiency
β	fuel/air ratio
ε_{r}	receiver's emittance

Acronyms

HRSG	heat recovery steam generator
GT	gas turbine
PTC	parabolic trough collector
COND	Condenser for cooling cycle
CP	circulation pump
d/a	deaerator
DNI	Direct Normal Irradiance, (kW/m^2)
DSG	Direct Steam Generation
EL	End Losses
EVAP	Evaporator for cooling cycle
G	Generator/power supply
GEN	Generator for cooling cycle
HEX1	heat exchanger 1
HEX2	heat exchanger 2
IAM	incidence Angle Modifier
SF	solar Field
ST	steam turbine
STIG	steam injection gas turbine
HTF	heat transfer fluid
NGG	natural gas generator
IE	incident energy
IEE	exergetic input

Subscripts

a	air
av	average value
c	cooling
cmp	compressor
comb	combined
f	fuel
in	inlet
o	ambient condition
out	outlet
R	receiver
s	steam
S	solar
tri	tri-generation

1 Introduction

Realizing the growing energy requirements of our country and meeting the same through a sustainable source, poses a big task for the energy society. In this direction increase of renewable energy share in the overall basket of power generation turns out to be the best solution. Among the numerous renewable energy resources, solar energy has gained the first place due to its free and ample nature of availability.

Generally, the trigeneration systems are known for their high efficiency and reliability. The integration of solar energy with trigeneration system is the noblest method of better energy harvesting. The trigeneration systems integrated with a solar energy system is the area of study of this work. Recent work done in this field is detailed as – (Tora and El-Halwagi, 2011) performed a preliminary design procedure for CCHP system using heat source fossil fuel and solar energy, also utilising process heat through absorption refrigeration. A solar cycle along with natural gas-fired combined-cycle plant was investigated by (Siva Reddy et al., 2012). For that, energy and exergy methods were used for comparative analysis of CCPP. It was observed that solar energy used for feedwater heater and LP steam generation is more effective based upon exergy analysis. Al-Sulaiman (2013) examined the solar field sizing and overall performance of various vapor cycles. The combined system consisted of PTCs and binary vapour cycle. This study revealed that by lowering the mass flow rate of HTF, the number of the solar collector required got reduced. Calise et al. (2014) studied the combination of sources especially water and renewable energy systems. They offered various multi-utilities at the same time, such as- electrical energy, thermal energy, cooling power, and domestic water. Cho et al. (2014) outlined the methods to perform energetic, exergetic, system optimization techniques upon CCHP systems. Their study also focused on the latest technological developments related to CCHP systems. Baniasad Askari et al. (2015) presented a techno-economic method for CCHP systems. Their study was based upon the analysis related to loss of power supply and cost of energy. It was observed that operational strategy changes with boiler and NGG fuel price. Baghernejad et al. (2015, 2016) completed thermodynamic analysis of SOFC based trigeneration system. They studied parameters, related to exergetic, economic, and environmental factors through multi-objective exergo-economic analysis. Angrisani et al. (2021) conducted a review of current methodologies and indices to analyse poly-generation system. Thereafter developed a correlation to accesses the feasibility of the system and classified various CCHP systems

as per the engine type, size, and usage. A procedure was identified which enlist such systems sequentially. The first level was applied for engine type, second for energy recovery components and third-level considered for energy storage and HTFs. Wang and Fu (2016) presented a proposed solar-based hybrid tri-generation system. Their system mentioned the methane chemical looping combustion technology used to generate electricity, cooling, and heating arrangement. The tri-generation system performance working upon the chemical looping combustion was analysed for flexible design. Further, the comparison was made related to energy and exergy efficiencies. Hands et al. (2016) performed analysis for a large-scale solar tri-generation system and discussed performance details for the operational gains. This system analysis offered various energy-related gains in a teaching institute building by solar-assisted desiccant cooling, heating, and hot water production.

Zhang et al. (2016) presented a system, in which solar energy with medium temperature was used to transform the chemical energy of biomass through the gasification process to biogas which was used as the fuel for the internal combustion engine to generate the electricity. Sharma and Singh (2016, 2017) and Sharma and Singh (2018) carried out various investigative analysis upon HRSG. They analysed conditions for varying flow and physical parameters for the energy and exergy methods of the combined cycle power plants. Adibhatla and Kaushik (2017) performed energy, exergy and economic analyses for solar assisted CCPPs. It was revealed that with solar field plant the output increased by 7.8% and the Levelized cost diminished by 7.4 to 6.7 cent/kWh.

Shukla et al. (2018) presented a thermodynamic analysis of the solar-powered Brayton cycle as the topping cycle with water/steam Rankine and Organic Rankine as bottoming cycles. The performance of the combined system was analysed for topping cycle pressure ratio as 31 and by using R245fa as organic fluid. Pavithran et al. (2021) and Sajwan et al. (2021) presented the hybrid power plant models on coal gasification model and waste heat recovery through super critical CO_2 respectively. Gang Lei et al. (2022) discussed about the performance of a hybrid nural based framework for alternative electricity pricing of smart grid.

The thermodynamic analysis and investigation of a medium capacity trigeneration system is proposed. The present novel trigeneration system is consisting of the solar cycle (PTC based), STIG turbine, bottoming cycle with fixed heating and cooling load. The effect of the combined system performance estimated through the mathematical model proposed and simulation is carried out and sensitivity of the system analysed. The typical trigeneration

system (at the baseline conditions) is also compared with the present system on the basis of workout, trigeneration efficiency and emissions rejected by the plant.

2 System Description

This integrated trigeneration system consists of the Solar Cycle (SC), Steam-Injected Gas Turbine (STIG) cycle, Heat Recovery Steam Generator (HRSG), Steam turbine cycle comprising heating and cooling provisions. The detailed layout of the STIG based trigeneration CCHP system is shown in Figure 1.

A Solar Field (SF) using Parabolic Trough Collector (PTC) has been joined with the Rankine cycle of the proposed system. The Rankine cycle's

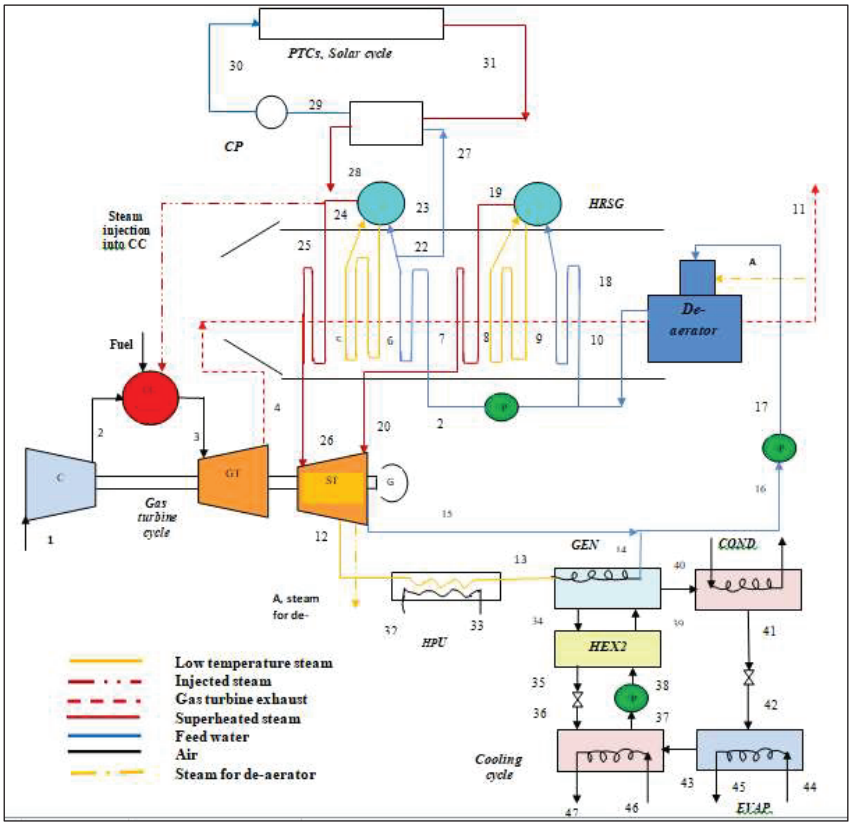

Figure 1 Detailed Layout of STIG based Trigeneration CCHP System.

HP feedwater absorbs the heat from the solar field (parabolic trough collectors and receiver arrangement). The parabolic trough collectors are positioned in the best-suited direction (north-south) in terms of the solar radiations. The sun tracking system follows the sun as per its movement from east to west direction. Direct Steam Generation (DSG) based on recirculation model has been considered for the present system. The separation of water from steam throughout the operation is done via steam separator placed at the end of the evaporator section of the collector field.

In the solar cycle, a pump is used to provide the required circulation throughout the collector field for absorbing heat energy for the bottoming cycle. The steam generated by the solar cycle is dry saturated steam (at 395°C) which is mixed with HP steam to add enhanced energy input to HP turbine. The proposed arrangement works as a tri-generation system (for power, heating and cooling arrangement). During solar hours, additional solar energy/heat is received through Solar Field which produces additional HP steam to supply to HP turbine. This additional steam flow is the added contribution of solar energy, other than waste heat utilization, in the steam turbine cycle. Moreover, bleed steam from the steam turbine under superheated state, is also taken for steam injection in the gas turbine. The steam turbine exhaust energy is further recovered by utilizing process heating, and cooling loads (fixed load) of the combined system.

2.1 Governing Equations

The mathematical equations for this work are taken from Baghernejad et al. (2015) and Duffie and Beckman (2013) and the solar collector based trigeneration system along with STIG are modeled as given under.

2.1.1 Solar system model

The energy balance for PTC based solar system is done through (Duffie and Beckman, 2013) using the following:

The collector useful energy rate is estimated as:

$$\dot{Q}_u = \dot{m}_r(C_{p,ro}T_{r,o} - C_{p,ri}T_{r,i}) \tag{1}$$

Where $\dot{m}_r$ oil mass flow rate circulated in the receiver, $C_{p,ro}, C_{p,ri}$ and $T_{r,o}, T_{r,i}$ shows the specific heats and temperatures at receiver, inlet, and outlet respectively.

The solar energy incident on the collector is given as:

$$\dot{Q}_i = DNI \cdot A_{ap} \cdot (\cos\theta)N \tag{2}$$

Where A_{ap} is aperture area, θ is the incidence angle, and N denotes the product of the number of collectors in a row, the number of modules in a collector and number of rows of collector array in the solar field, DNI represents the direct normal irradiance considered in a plane normal to the sun.

$$A_{ap} = (w - D_{cod})l \tag{3}$$

Where *w*, represents the collector width, D_{cod}, represents the cover outer diameter, and *l* is the collector length.

The exergetic solar energy input to parabolic trough is given as:

$$E_{\varkappa_i} = \dot{Q}_i \left[1 - \frac{4}{3}\left(\frac{T_0}{T_s}\right) + \frac{1}{3}\left(\frac{T_0}{T_s}\right)^4\right] \tag{4}$$

Where T_s and T_o are the black body surface and ambient temperatures ($T_s = 5800$ K is black body temperature of the sun).

The solar energy absorbed by the receiver is estimated as:

$$\dot{Q}_a = DNI \cdot IAM \cdot A_a\, N \cdot \gamma_r \cdot \tau_g \cdot \alpha_a \cdot IF \cdot \eta_{sd} \cdot EL \tag{5}$$

Where 'γ_r' represents the mirror's surface reflectivity, 'τ_g' is the receiver glass transmissivity, 'α_a' is the absorptivity of absorber surface, 'IF' is the intercept factor, 'η_{sd}' shading factor and 'EL' is the end loss factor.

The trough collector Incidence Angle Modifier (IAM) is given by:

$$IAM = cos\theta - 2.859621 \times 10^{-5} \cdot (\theta)^2 - 5.25007 \times 10^{-4}(\theta) \tag{6}$$

The End Losses (EL) factor Reddy et al. (2012) is estimated as:

$$EL = 1 - \frac{f}{L}\, tan\theta \tag{7}$$

Where *f* is the 'collector' focal length.

The solar collector exergy is given by:

$$E_{xe} = \dot{Q}_a \left(1 - \frac{T_o}{T_r}\right) \tag{8}$$

Where 'T_r' is the receiver temperature in K.

The useful energy gained by the solar collector,

$$\dot{Q}_u = F_r(\dot{Q}_a - U_L\, A_r(T_i - T_e)) \tag{9}$$

$$A_r = \pi\, D_i\, l \tag{10}$$

The collector heat removal factor is estimated as,

$$F_r = \frac{\dot{m}_f\, C_p}{U_L\, A_r}\left[1 - e^{-\left(\frac{U_L A_r F'}{\dot{m}_f\, C_p}\right)}\right] \tag{11}$$

The collector efficiency factor is related as,

$$F' = \frac{U_o}{U_L} \tag{12}$$

The solar collector heat loss coefficient is,

$$U_L = \left[\frac{A_r}{(h_{c,ca} + h_{r,ca})\, A_c} + \frac{1}{h_{r,cr}}\right]^{-1} \tag{13}$$

The ambient state and the cover radiation heat transfer coefficient is estimated as,

$$h_{r,ca} = \varepsilon_{cv}\sigma(T_c + T_a)({T_c}^2 + {T_a}^2) \tag{14}$$

Where, ε_{cv} is the emittance of the cover and σ is the Stefan-Boltzmann coefficient.

The receiver and the cover radiation heat transfer coefficient is given by,

$$h_{r,cr} = \frac{\sigma(T_c + T_{r,av})({T_c}^2 + {T_{r,\,av}}^2)}{\frac{1}{\varepsilon_r} + \frac{A_r}{A_c}\left(\frac{1}{\varepsilon_{cv}} - 1\right)} \tag{15}$$

Where the receiver's emittance is 'ε_{r}' and the 'av' is used for representing average value.

The cover and ambient convection heat loss coefficient is defined as,

$$h_{c,ca} = \frac{Nu \cdot k_{air}}{D_{c,o}} \tag{16}$$

Where *Nu* and k_{air} is the Nusselt number and thermal conductivity of air respectively.

The overall heat transfer coefficient for the surroundings can be given as,

$$U_o = \left[\frac{1}{U_L} + \frac{D_{r,o}}{h_{c,rin}\, D_{r,i}} + \left(\frac{D_{r,o}}{2k_r} ln\left(\frac{D_{r,o}}{D_{r,i}}\right)\right)\right]^{-1} \tag{17}$$

Table 1 Parabolic trough collector configurations (Baghernejad et al., 2015, 2016)

Chosen Parameters	Value (Units)	Chosen Parameters	Value (Units)
Aperture area, A_{ap}	545 m^2	HEC transmittance	0.96
Collector aperture, w	5.76 m	Mirror reflectivity, ρ	0.94
Heat collection element (HCE) diameter, $D_{c,o}$	0.07 m	Single Collector Length	12.27 m
HCE absorptivity, α	0.96	Concentration ratio	82
Emittance of the receiver, ε	0.15	Optical efficiency/ Receiver's efficiency, η_r	80%
No. of solar collector	10	Average focal distance	0.94m
Receiver inner diameter	0.066 m	Receiver outer diameter	0.07 m
Shading Factor	0.98	Glass cover transmittance	0.96
DNI (used for hot summer in Delhi region, India)	–	Intercept factor	0.92

2.1.2 Combined STIG based cooling, heating and power model

The energy balance equations for the proposed model consisting of gas mixture heat capacity estmation, than total energy available, mass of steam injected, overall power developed. The performance parameters such as power developed, trigeneration system efficiency and amount of carbon foot print were calculated.

The specific heat for the mixture of gases is related as the sum specific heats of each component and their mass fractions (y_i).

$$C_p(T) = \sum_{i=1}^{n} y_i C_{pi}(T) \tag{18}$$

The specific heat for actual gas mixture is taken from Moran and Shapiro [14] and given as:

$$C_p = \frac{R}{M}(\alpha + \beta T + \gamma T^2 + \delta T^3 + \varepsilon T^4) \tag{19}$$

Where, 'R' represents the universal gas constant, 'M' represents the molar mass of the gas, and α, β, γ, ε and δ are the constants for various gases.

The total energy input (q_{in}) to the tri-generation system comprising the energy from the fuel and solar thermal energy,

$$\dot{q}_{in} = \dot{q}_{ng} + \dot{q}_{solar} \tag{20}$$

Where q_{ng} and q_{solar} are the energy obtained from natural gas and through the solar cycle respectively.

Table 2 The chosen baseline parameters for the trigeneration system, Sharma and Singh (2016, 2017)

Chosen Parameters	Value Taken
Combustion chamber efficiency	95%
Compressor efficiency	90%
Cooling load / Electricity generated	3–5%
Cycle pressure ratio	12
Heating load/Electricity generated	2–4%
Mass flow rate of air	60 kg/s
Mass flow rate of fuel (without steam injection)	2.5 kg/s
Mechanical efficiency	95%
Natural gas, LHV	45.42 MJ/kg
Solar share	8–12%
Steam generation pressure, HP	84 bar
Steam generation pressure, LP	9 bar
Steam generation temperature, HP	780 K
Steam generation temperature, LP	666 K
Steam injection pressure	12 bar
Steam injection temperature	1400 K
Turbine efficiency	90%
Turbine inlet temperature	1400 K

As the steam injection is also used in the combustion chamber, the energy balance of the combustion chamber provides fuel/air ratio (β), can be estimated as –

$$\beta = \frac{(h_{3,a} - h_{2,a}) + \frac{\dot{m}_s}{\dot{m}_a}(h_{3,steam} - h_{in,\ steam})}{LCV \cdot \eta_{cc} - (1+f)Dh_3 - h_{3,g}} \tag{21}$$

Where, $h_{2,a}$ and $h_{3,a}$ specific enthalpies of air at point 2 and 3 respectively, $h_{in,steam}$ and $h_{3,steam}$ specific enthalpies of steam at point 24 and 3 respectively and $h_{3,g}$ is the specific enthalpy of the exhaust gases.

The power generated by the steam injected gas turbine, can be estimated as:

$$\begin{aligned}\dot{W}_{gt} = (\dot{m}_a + \dot{m}_f)(h_{3,g} - h_{4,g}) + \dot{m}_s(h_{s,tit} - h_{s,t4}) \\ - \dot{m}_a(h_{2,a} - h_{1,a})\end{aligned} \tag{22}$$

The net power generated in the tri-generation system (power generated by the steam injected gas turbine cycle and steam turbine cycle) is estimated as:

$$\dot{W}_{net} = \dot{W}_{gt} + \dot{W}_{st} \tag{23}$$

The tri-generation system overall efficiency can be estimated as:

$$\eta_{tri} = \frac{\dot{W}_{net} + \dot{q}_h + \dot{q}_c}{q_{in}} \tag{24}$$

Where, $\dot{W}_{net}$ represents net power generated, $\dot{q}_h$ is the heating load, $\dot{q}_c$ is the cooling load, and total energy input in the trigeneration system.

The trigeneration system, CO_2 emission rate of can be estimated as:

$$emi_{CO2} = \frac{\dot{m}_{CO2}}{\dot{W}_{net} + \dot{q}_h + \dot{q}_c} 3600 \tag{25}$$

The emission rate is the amount of CO_2 released per unit energy developed by the trigeneration system.

3 Results and Discussion

The primary attention in the analysis of the trigeneration system is based on two important considerations. First is to observe the effect of the conversion of solar energy to thermal power generation and second is to analyze the effect of steam injection in gas turbine for a trigeneration system.

The results obtained for the integrated solar-based trigeneration systems are presented here for the important operating parameters. The thermodynamic, and environment analysis of the system for the important operating parameters are discussed below.

The DNI variations taken for the analysis are a variation of the peak summer radiations in Delhi NCR region, India.

Figure 2 shows the effect of variation in the incident energy and exergetic input with direct normal irradiance (DNI). It is observed that the incident energy falling on the parabolic trough collector increases with DNI and number of rows.

The exergetic input on the parabolic surface indicates the quality of energy absorbed by it considering all losses through the receiver. The increase in the number of rows enhances the amount of energy at the receiver's pipe. The percent variations observed by the incident energy and exergetic input are around 7%. It provides the correct evaluation of the physical components of the solar cycle for further utilization in the trigeneration system.

The variation of exergetic input on PTC and exergy on the receiver pipe with DNI is shown in Figure 3. The result obtained depicts that the receiver pipe exergy follows the same trend as exergetic input. However, in absolute

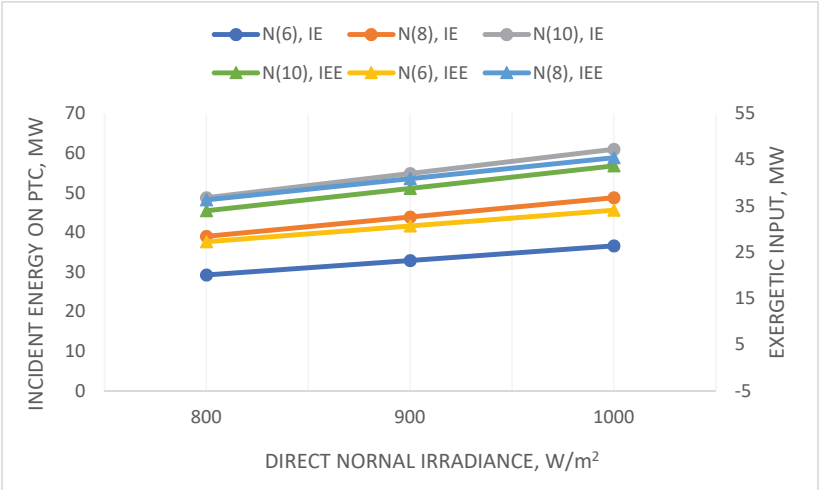

Figure 2 Variation of incident energy and exergetic input with direct normal irradiance.

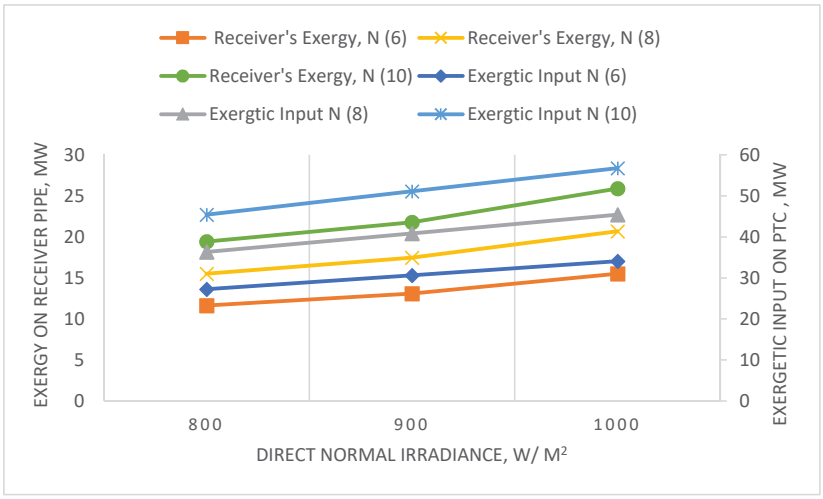

Figure 3 Variation of receiver's exergy and exergetic input with direct normal irradiance (DNI).

values, the difference in the values of the exergies at two surfaces are almost constant. However, this decrease in exergtic input and receiver exergy varying in the range of 50–60% shows the amount of exergy loss associated with various losses. It also observed that when the direct normal irradiance varies

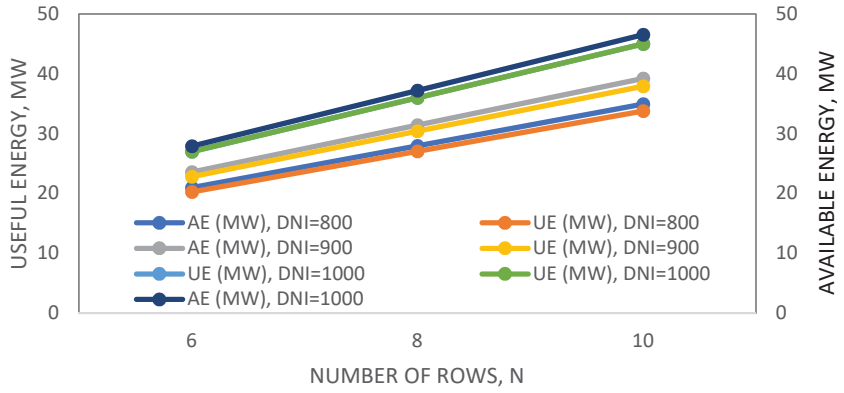

Figure 4 Variation of useful energy and available energy with the number of rows.

from 800–1000 W/m^2, the exergetic input and receiver's exergy varies by around 25% and 33%, respectively. These variations are due to different kind of losses on the respective surfaces.

Figure 4 describes the variation of useful energy and available energy with the number of rows. The useful energy obtained at the receiver's pipe is the available energy obtained after considering radiation, convection, and conduction losses. The result shows that as the number of rows increases, the useful energy, and available energy increases. However, it is also affected by the factors incorporated for the different losses. These losses produce a variation of around 5% from the useful energy and available energy on the receiver's surface, respectively.

The variation of trigeneration efficiency with GT (gas turbine) pressure ratio is described in Figure 5. Here it is depicted that for different DNIs and number of rows, the trigeneration efficiency increases with GT pressure ratio. The trigeneration efficiencies of the stated system show a considerable increase at a more significant number of rows. While the increase in trigeneration efficiencies is not substantial for pressure ratios, this varies around 0.4% for the higher-pressure ratio at a fixed number of rows and DNI. The more significant number of rows and higher DNI reveals around 14–16% variations.

Figure 6(a) reveals the variation of trigeneration efficiency with turbine inlet temperature for the different number of rows and DNI (800 W/m^2). It is observed that trigeneration efficiency increases for the different number of rows for the higher gas turbine inlet temperature. The trigeneration efficiency increases by around 15% for the number of rows from 6 to 8, as evident from

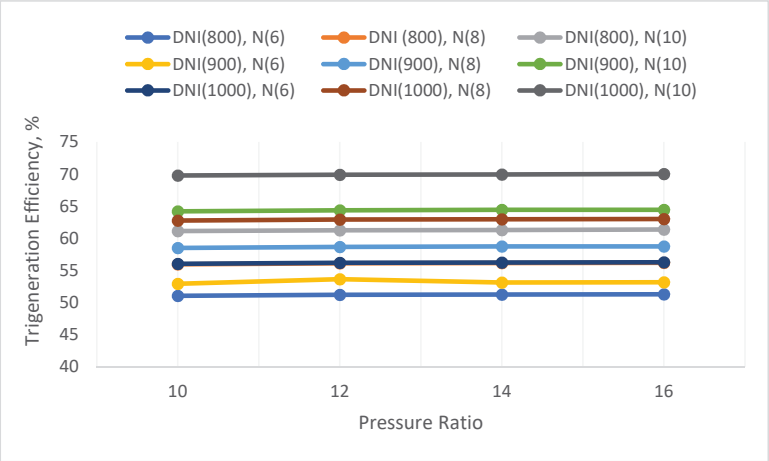

Figure 5 Variation of trigeneration efficiency with pressure ratio for different DNI and no. of rows.

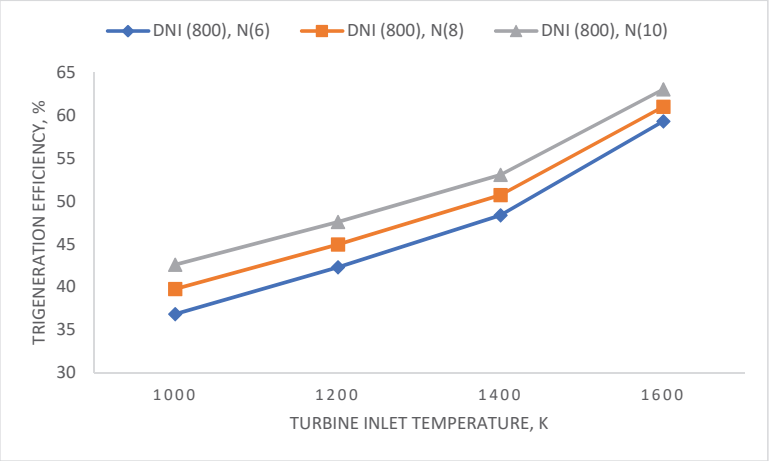

Figure 6(a) Variation of trigeneration efficiency with turbine inlet temperature for different no. of rows (DNI = 800 W/m^2).

the graphical results. The trigeneration efficiency of the stated system shows a considerable increase at higher TIT for the number of rows.

The variation of the plant trigeneration efficiency with turbine inlet temperature for the fixed radiations (DNI = 900 W/m^2) shown in Figure 6(b). These results show that the increase in numbers of rows from 6 to 8 at fixed

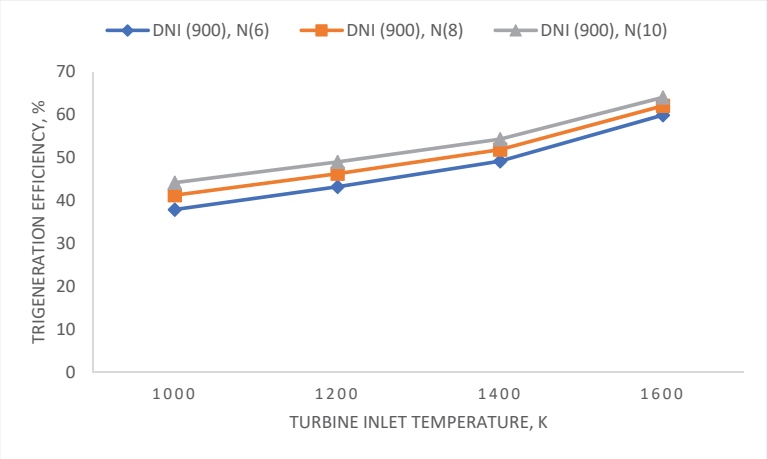

Figure 6(b) Variation of trigeneration efficiency with turbine inlet temperature for different no. of rows (DNI = 900 W/m^2).

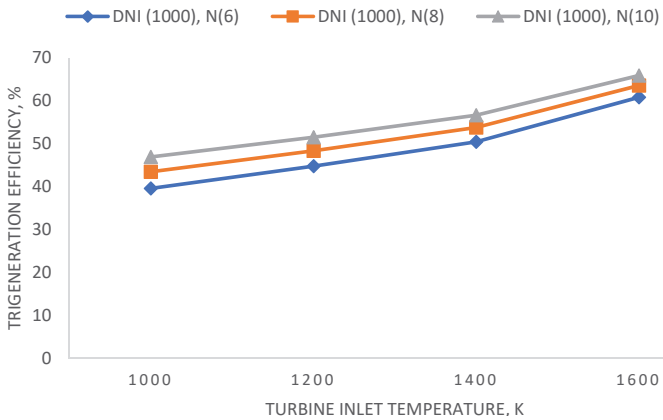

Figure 6(c) Variation of trigeneration efficiency with turbine inlet temperature for different no. of rows (DNI = 1000 W/m^2).

DNI increases efficiency by 17%. Further, the increase in plant efficiency is comparatively higher for turbine inlet temperature for the considered range.

The variation of the plant trigeneration efficiency with turbine inlet temperature for the fixed radiations (DNI = 1000 W/m^2) shown in Figure 6(c). These results show that with an increase in numbers of rows from 6 to 8 at fixed DNI, increases efficiency by 19%. Moreover, this increase in plant efficiency is comparatively higher for turbine inlet temperature within

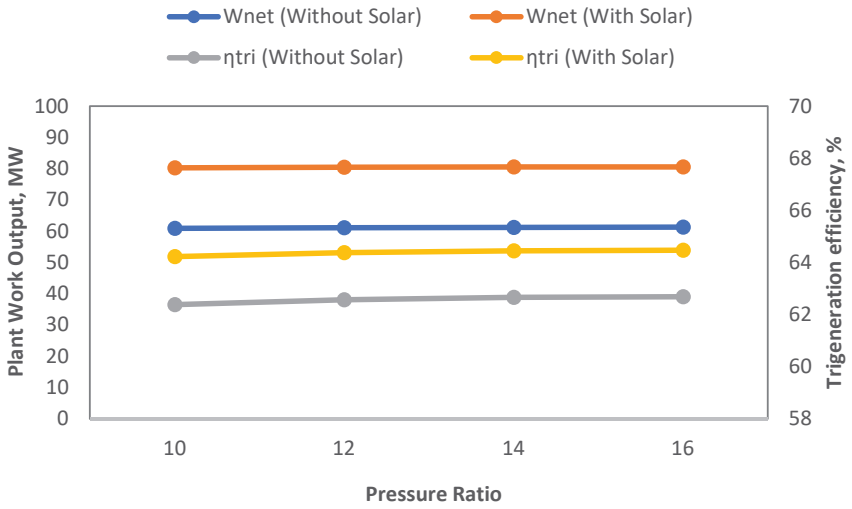

Figure 7 Variation of plant work output and trigeneration efficiency for trigeneration system (with and without solar field).

the considered range. It depicts that TIT is the crucial parameter for the integrated system for fixed DNI and number of rows. It shows the increase in trigeneration efficiency by around 50% for these three cases, as evident in Figures 6(a), 6(b), and 6(c).

Figure 7 shows the variation of trigeneration efficiency and plant work output variation with pressure ratio with and without solar-assisted system. The effect of pressure ratio change on plant performance indicates little variations in plant work output and trigeneration efficiency. These variations in efficiency and plant work output are around 0.5% and 0.4% with gas turbine pressure ratio. Therefore, the net-work output and trigeneration efficiency show a lesser effect on cycle pressure. However, the effect on work output and trigeneration efficiency is comparatively higher by around 30% and 3% respectively in the cycle with the solar system as compared to the cycle without the solar system in the trigeneration.

The trigeneration efficiency and plant work output variation with turbine inlet temperature are shown in Figure 8 (with and without solar-assisted system) trigeneration system.

The effect of turbine inlet temperature indicates considerable variation in net work out of trigeneration system. The effect on work output and trigeneration efficiency with TIT is compared for the with and without solar cycle trigeneration plant. The significant changes are observed as the

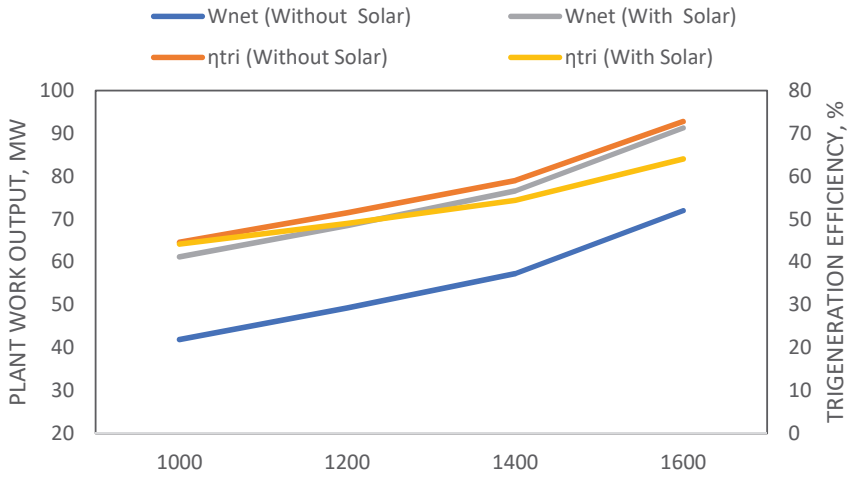

Figure 8 Variation of plant work output and trigeneration system efficiency with and without solar integration.

estimated work output in an arrangement without solar cycle increased by around 70% for the considered range with STIG cycle. The work output with solar cycle also increases with TITs, and this increase is around 50%. The trigeneration plant efficiency with and without solar cycle improved by 60% and 40% respectively for the considered TIT range. Further, it is observed that at the fixed TIT, the improvement in work output (for the arrangements with and without a solar cycle) is around 20–25%. Whereas, the trigeneration plant efficiency for the arrangements (with and without solar cycle) decreases around 2–10% for the considered TITs.

The variations in carbon footprint with the change in GT cycle pressure ratio with and without the solar cycle of the trigeneration system shown in Figure 9. The carbon footprint decreases marginally as the pressure ratio increases for all cases i.e., with and without solar cycle. The decrease in carbon footprints by around 20% in the arrangement with the solar cycle as the overall energy generation/utilization improves with reduced fuel (fossil) consumption.

The variation of carbon footprint with GT pressure ratio is shown in Figure 10 (for the arrangements with and without solar-assisted) trigeneration system. The carbon footprint decreases considerably with the higher TITs in case of the arrangement with the solar-assisted trigeneration system. It is evident from the results that there occurs the reduction in carbon footprints with higher TITs by around 30–35% in the case of the solar cycle.

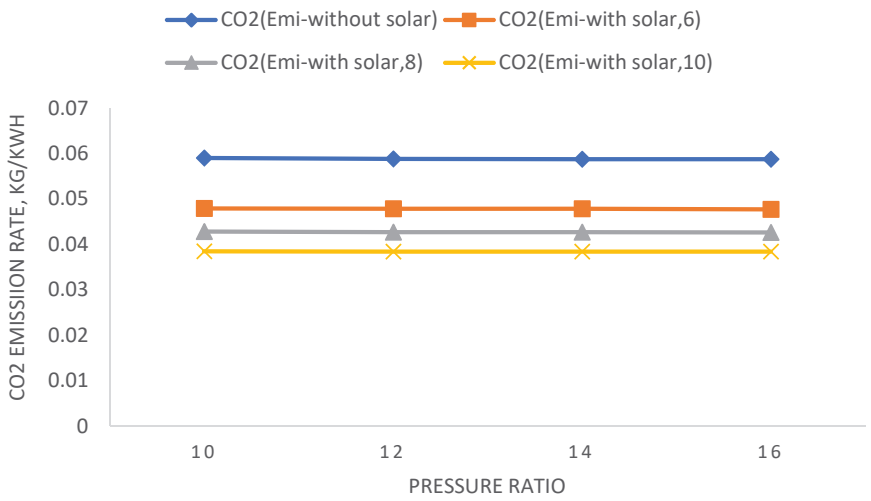

Figure 9 Effect of CO_2 emission with pressure ratio for trigeneration system (with solar and without solar)

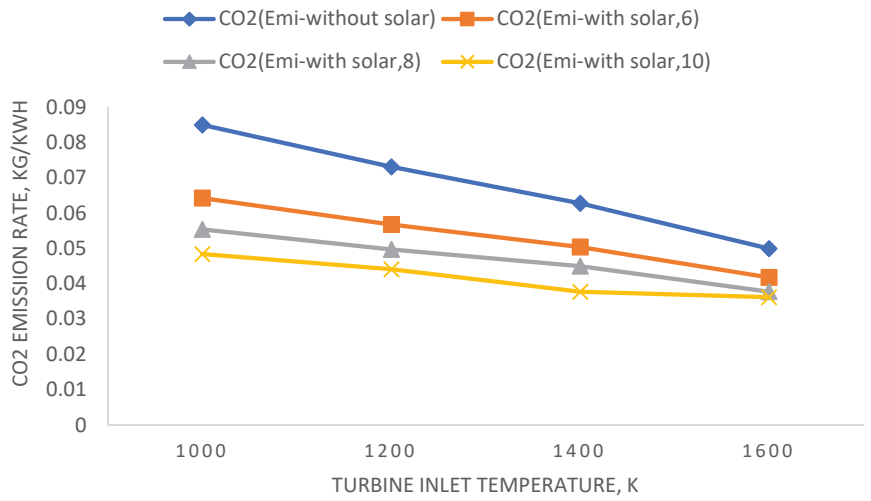

Figure 10 Effect of CO_2 emission with turbine inlet temperature for trigeneration systems with solar and without solar.

The variations in work output and trigeneration efficiency with GT pressure ratio (with and without STIG) shown in Figure 11. The results reveal similar trends for work output and trigeneration efficiency for the two cases. The work output and trigeneration efficiency with STIG increases at a low

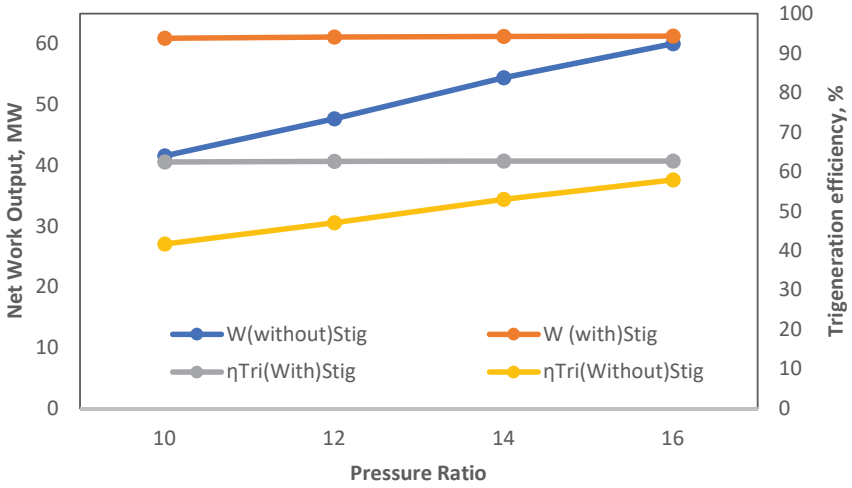

Figure 11 Variation of net-work output and trigeneration efficiency with pressure ratio for trigeneration systems (with and without STIG).

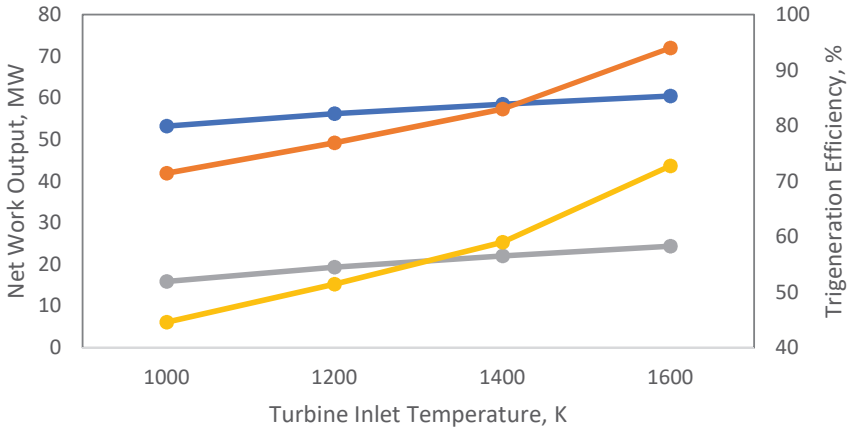

Figure 12 Variation of net-work output and trigeneration efficiency with turbine inlet temperature for trigeneration systems (with and without STIG).

rate of around 0.5%. Whereas the work output and the trigeneration efficiency in the arrangement without the STIG system increase by around 40–44% respectively.

Figure 12 depicts the variations in network output and trigeneration efficiency with turbine inlet temperature (with and without STIG). The results show similar trends for work output and trigeneration efficiency for the

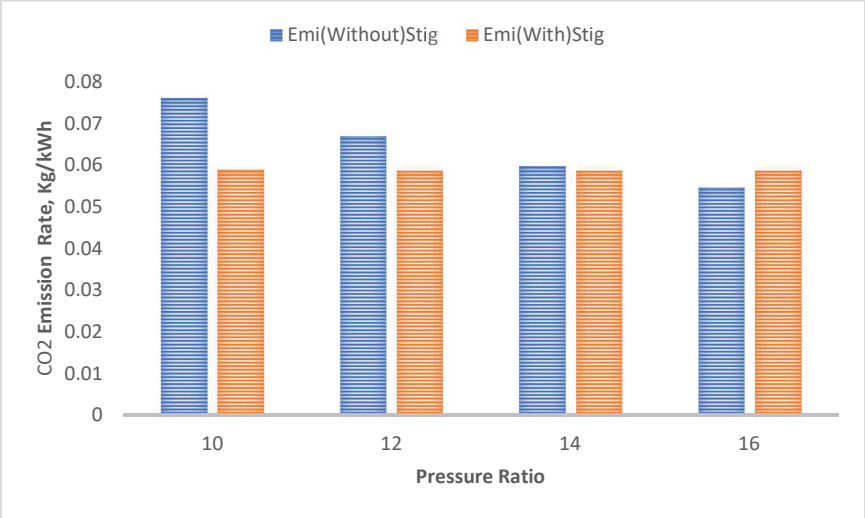

Figure 13 Variation of CO_2 emissions with pressure ratio for trigeneration systems with and without steam injection.

two cases (with and without STIG). The work output and trigeneration efficiency with STIG increases substantially around 60% and 70% respectively with higher TIT whereas the work output and the trigeneration efficiency in the arrangement without STIG system increase around 7% and 13.5% respectively with higher TIT.

The CO_2 emission is one of the crucial parameters to be analyzed as it will give the correct estimate of the required size of the plant. The result of analysis for the fixed TIT, the effect on CO_2 emissions with pressure ratio for the trigeneration systems with and without steam injection in gas turbine cycle is shown in Figure 13. It is observed that for higher pressure ratio, the steam injection in gas turbine cycle yields around 0.5% carbon footprint. It is also evident that for higher pressure ratio in the arrangement without steam injection in gas turbine cycle, the carbon footprint reduced by around 25%. The leading cause of comparatively low carbon footprint is due to steam injection in the combustion zone, which reduces the peak flame temperature and thereby decrease the CO_2 emissions.

Figure 14 shows the variations of CO_2 emissions with turbine inlet temperature for the trigeneration systems with and without steam injection in gas turbine cycle. It observed that for higher turbine inlet temperature in the arrangement with the steam injected gas turbine cycle, the carbon footprint

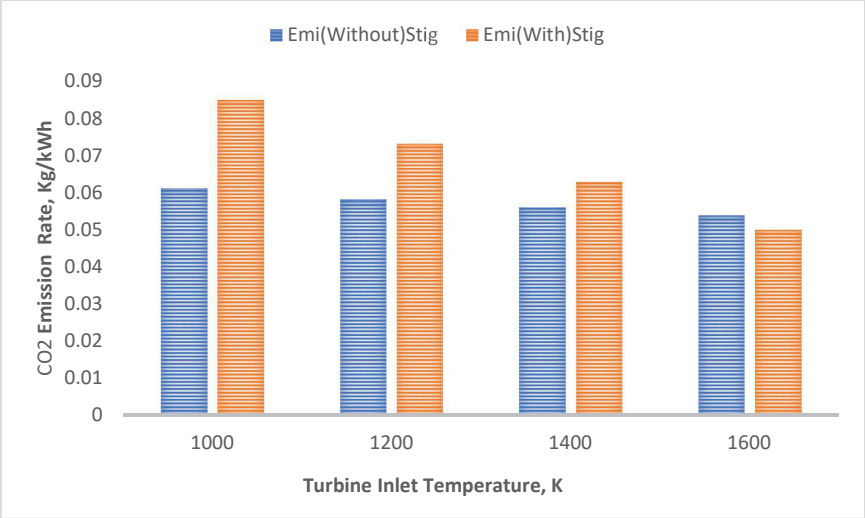

Figure 14 Variation of CO_2 emissions with turbine inlet temperature for trigeneration systems with and without steam generation.

reduces by around 40% and in the arrangement without steam injection by 10%. The results obtained are compared with (Baghernejad et al., 2015) and are found to be in coherence and show the reduction in the carbon footprint by around 25%.

4 Conclusions

The analysis of the results obtained for the parametric investigations on the solar cycle based trigeneration system leads to the following conclusions.

- The incident energy falling to the PTCs and the useful energy for the steam generation in the bottoming cycle shows 25–35% deviations in the energy available on the collector and receiver surface.
- The comparison of the trigeneration system with and without solar cycle shows improvement in work output, and trigeneration efficiency and the emission contents reduced from 20–30% for the higher GT pressure ratio and TITs.
- The effect of steam injection on the trigeneration system in terms of work output improves trigeneration efficiency, and emission gets reduced from 10–40% for the higher GT pressure ratio and TITs.

- New challenges of the current scenario such as thermal efficiency, work output and carbon foot print are highlighted by present analysis. The results inform that the useful energy captured by solar system for STIG based combined cooling, heatng and power system shows improvement. The sensitivity of proposed system has been chaecked and its parameters are compared with extsing system which will be highly useful in designing of a combined power plants.

References

Adibhatla, Sairam, and S. C. Kaushik. 2017. "Energy, Exergy and Economic (3E) Analysis of Integrated Solar Direct Steam Generation Combined Cycle Power Plant." Sustainable Energy Technologies and Assessments 20 (April). Elsevier: 88–97. doi:10.1016/J.SETA.2017.01.002.

Al-Sulaiman, Fahad A. 2013. "Energy and Sizing Analyses of Parabolic Trough Solar Collector Integrated with Steam and Binary Vapor Cycles." Energy 58 (September). Pergamon: 561–570. doi:10.1016/J.ENERGY.2013.05.020.

Angrisani, G, A Akisawa, E Marrasso, ... C Roselli – Energy Conversion and, and undefined 2016. 2021. "Performance Assessment of Cogeneration and Trigeneration Systems for Small Scale Applications." Elsevier. Accessed December 28. https://www.sciencedirect.com/science/article/pii/S0196890416302394.

Baghernejad, A., M. Yaghoubi, and K. Jafarpur. 2015. "Optimum Power Performance of a New Integrated SOFC-Trigeneration System by Multi-Objective Exergoeconomic Optimization." International Journal of Electrical Power & Energy Systems 73 (December). Elsevier: 899–912. doi:10.1016/J.IJEPES.2015.06.017.

Baghernejad, A., M. Yaghoubi, and K. Jafarpur. 2016. "Exergoeconomic Optimization and Environmental Analysis of a Novel Solar-Trigeneration System for Heating, Cooling and Power Production Purpose." Solar Energy 134 (September). Pergamon: 165–179. doi:10.1016/J.SOLENER.2016.04.046.

Baniasad Askari, I., M. Oukati Sadegh, and M. Ameri. 2015. "Energy Management and Economics of a Trigeneration System Considering the Effect of Solar PV, Solar Collector and Fuel Price." Energy for Sustainable Development 26 (June). Elsevier: 43–55. doi:10.1016/J.ESD.2015.03.002.

Calise, Francesco, Massimo Dentice d'Accadia, and Antonio Piacentino. 2014. "A Novel Solar Trigeneration System Integrating PVT (Photovoltaic/Thermal Collectors) and SW (Seawater) Desalination: Dynamic Simulation and Economic Assessment." Energy 67 (April). Pergamon: 129–148. doi:10.1016/J.ENERGY.2013.12.060.

Cho, Heejin, Amanda D. Smith, and Pedro Mago. 2014. "Combined Cooling, Heating and Power: A Review of Performance Improvement and Optimization." Applied Energy 136 (December). Elsevier: 168–185. doi:10.1016/J.APENERGY.2014.08.107.

Duffie, J.A, and Beckman. 2013. Solar Engineering of Thermal Processes. John Wiley & Sons.

Hands, Stuart, Subbu Sethuvenkatraman, Mark Peristy, Daniel Rowe, and Stephen White. 2016. "Performance Analysis & Energy Benefits of a Desiccant Based Solar Assisted Trigeneration System in a Building." Renewable Energy 85 (January). Pergamon: 865–879. doi:10.1016/J.RENENE.2015.07.013.

Lei, G., Xu, C., Chen, J., Zhao, H. and Parvaneh, H., 2022. Performance of a Hybrid Neural-Based Framework for Alternative Electricity Price Forecasting in the Smart Grid. Distributed Generation & Alternative Energy Journal, pp. 405–434. https://doi.org/10.13052/dgaej2156-3306.3731

Pavithran, A., Sharma, M. and Shukla, A.K., 2021. Oxy-fuel Combustion Power Cycles: A Sustainable Way to Reduce Carbon Dioxide Emission. Distributed Generation & Alternative Energy Journal, pp. 335–362. https://doi.org/10.13052/dgaej2156-3306.3641

Sajwan, K., Sharma, M. and Shukla, A.K., 2020. Performance Evaluation of Two Medium-Grade Power Generation Systems with CO2 Based Transcritical Rankine Cycle (CTRC). Distributed Generation & Alternative Energy Journal, pp. 111–138. https://doi.org/10.13052/dgaej2156-3306.3522

Sharma, Meeta, and Onkar Singh. 2016. "Exergy Analysis of Dual Pressure HRSG for Different Dead States and Varying Steam Generation States in Gas/Steam Combined Cycle Power Plant." Applied Thermal Engineering 93 (January). Pergamon: 614–622. doi:10.1016/J.APPLTHERMALENG.2015.10.012.

Sharma, Meeta, and Onkar Singh. 2018. "Energy and Exergy Investigations Upon Tri-Generation Based Combined Cooling, Heating, and Power (CCHP) System for Community Applications." ASME 2017 Gas Turbine India Conference, GTINDIA 2017 2 (February). American Society of Mechanical Engineers Digital Collection. doi:10.1115/GTINDIA2017-4559.

Shukla, Anoop Kumar, Achintya Sharma, Meeta Sharma, and Gopal Nandan. 2018. "Thermodynamic Investigation of Solar Energy-Based Triple Combined Power Cycle." https://doi.org/10.1080/15567036.2018.1544 99541(10). Taylor & Francis: 1161–1179. doi:10.1080/15567036.2018. 1544995.

Siva Reddy, V., S. C. Kaushik, and S. K. Tyagi. 2012. "Exergetic Analysis of Solar Concentrator Aided Natural Gas Fired Combined Cycle Power Plant." Renewable Energy 39(1). Pergamon: 114–125. doi:10.1016/J. RENENE.2011.07.031.

Tora, Eman A., and Mahmoud M. El-Halwagi. 2011. "Integrated Conceptual Design of Solar-Assisted Trigeneration Systems." Computers and Chemical Engineering 35(9): 1807–1814. doi:10.1016/j.compchemeng. 2011.03.014.

Wang, Jiangjiang, and Chao Fu. 2016. "Thermodynamic Analysis of a Solar-Hybrid Trigeneration System Integrated with Methane Chemical-Looping Combustion." Energy Conversion and Management 117 (June). Pergamon: 241–250. doi:10.1016/J.ENCONMAN.2016.03.039.

Zhang, Xiaofeng, Hongqiang Li, Lifang Liu, Rong Zeng, and Guoqiang Zhang. 2016. "Analysis of a Feasible Trigeneration System Taking Solar Energy and Biomass as Co-Feeds." Energy Conversion and Management 122 (August). Pergamon: 74–84. doi:10.1016/J.ENCONMAN.2 016.05.063.

Biographies

Meeta Sharma is working as an Associate Professor in the Mechanical Engineering Department, Amity University, Noida. She is Ph.D from Dr. A.P.J. Abdul Kalam Technical University, Lucknow, India. Her area of interest are Hybrid power plants, Renewable energy, Waste heat recovery systems, Heat transfer and Applied thermodynamics.

Onkar Singh is an Indian Professor of Mechanical Engineering, Harcourt Butler Technological University, Kanpur and Vice Chancellor of Veer Madho Singh Bhandari Uttarakhand Technical University, Dehradun.
http://dronkarsingh.in

Anoop Kumar Shukla is currently an assistant professor in the Department of Mechanical Engineering Amity University Noida India. He received his master and doctoral degree from Harcourt Butler Technological Institute Kanpur. His research interest concern energy conversion and thermal management, hybrid power cycles, Biofuels, gas turbine cooling, and advanced thermodynamics.